

Seismic performance evaluation of a multi-slit damper

Asad Naeem, Jinkoo Kim*

Department of Civil and Architectural Engineering, Sungkyunkwan University, Suwon, Republic of Korea



ARTICLE INFO

Keywords:

Hysteretic dampers
Slit dampers
Nonlinear dynamic analysis
Seismic performance
Seismic retrofit

ABSTRACT

This research proposed a new displacement-dependent energy dissipation device for seismic protection of framed structures. The multi-slit damper (MSD) was developed by combining weak and strong steel slit dampers in series. The MSD has two stages of energy dissipation with different yielding forces and stiffnesses: for low to medium earthquakes, the weak-slit damper yields and dissipate seismic energy. For stronger earthquakes, further deformation in the weak slit damper is restrained and the strong-slit damper begins to dissipate the energy. Cyclic loading test of a prototype MSD was carried out to evaluate the seismic energy dissipation capacity. Finite element analysis of the test specimen was also carried out for validation of the test results. A simplified numerical model of the MSD was developed in the framework of commercially available structural analysis software. The seismic performance of a reinforced concrete (RC) model structure retrofitted with the MSD was investigated and was compared with that of the model structure retrofitted with conventional slit dampers. The experimental and analysis results showed that the MSD is effective in reducing seismic response of framed structures.

1. Introduction

The hysteretic or metallic yielding dampers enhance seismic performance of a structure by dissipating earthquake-induced energy through stable hysteretic behavior. The application of yielding devices for the seismic retrofit of existing structures has increased due to their ease of manufacture and installation. The introduction of suitable design guidelines and specifications has also contributed to the spread of energy dissipation devices. Whittaker et al. [1] and Tsai et al. [2] investigated the seismic performance of steel plate added damping and stiffness (ADAS) elements and triangular plate energy absorbers (TADAS), respectively, which dissipate seismic energy through bending of steel plates. Kobori et al. [3] proposed energy-absorbing devices made of steel plates with vertical openings, which dissipate seismic energy through in-plane hysteretic behavior. Chan and Albermani [4] proposed the steel slit damper fabricated from a standard structural wide-flange section with a number of slits cut from the web, and verified its energy absorbing capacity through experiments. Benavent-Climent [5] investigated the use of the web of standard wide-flange sections subjected to out of plane bending as energy-dissipating devices for seismic applications. Köken and Köroğlu [6] developed a slit steel damper system for energy dissipation at beam-to-column connections of steel frames. Analytical and experimental investigations of various hysteretic steel damper for building structure are also performed in

[7–9].

Steel slit dampers are considered as an efficient seismic protection device for structures in the field of earthquake engineering. However their energy dissipation capacity is completely lost when the slit columns are fractured at large displacement. Several studies have been carried out to enhance its seismic performance. Lee and Kim [10] developed hybrid damping devices by combining steel slit and rotational friction dampers connected in parallel, and showed that the hybrid dampers are especially effective in reducing seismic responses for small to medium earthquakes, compared with slit or friction dampers with the same yield strength. Kim and Shin [11] studied the seismic loss assessment of a structure retrofitted with slit-friction dampers through test and analysis. The seismic performance of a self-centering hybrid slit damper with shape memory alloy bars was investigated by Naeem et al. [12,13]. The hybrid slit dissipation device turned out to be effective in reducing both the earthquake-induced maximum and residual displacements of a structure.

This study aims to develop a multi-slit damper (MSD) in which weak and strong slit dampers are connected in series. The proposed damper consists of steel slit dampers with two different stiffnesses and yield strengths. During low to medium earthquakes, the weak slit damper is activated while the strong slit damper remains elastic. For severe earthquakes, both the weak and strong dampers act together to dissipate large seismic energy. When the displacement of the weak slit

* Corresponding author.

E-mail address: jkim12@skku.edu (J. Kim).

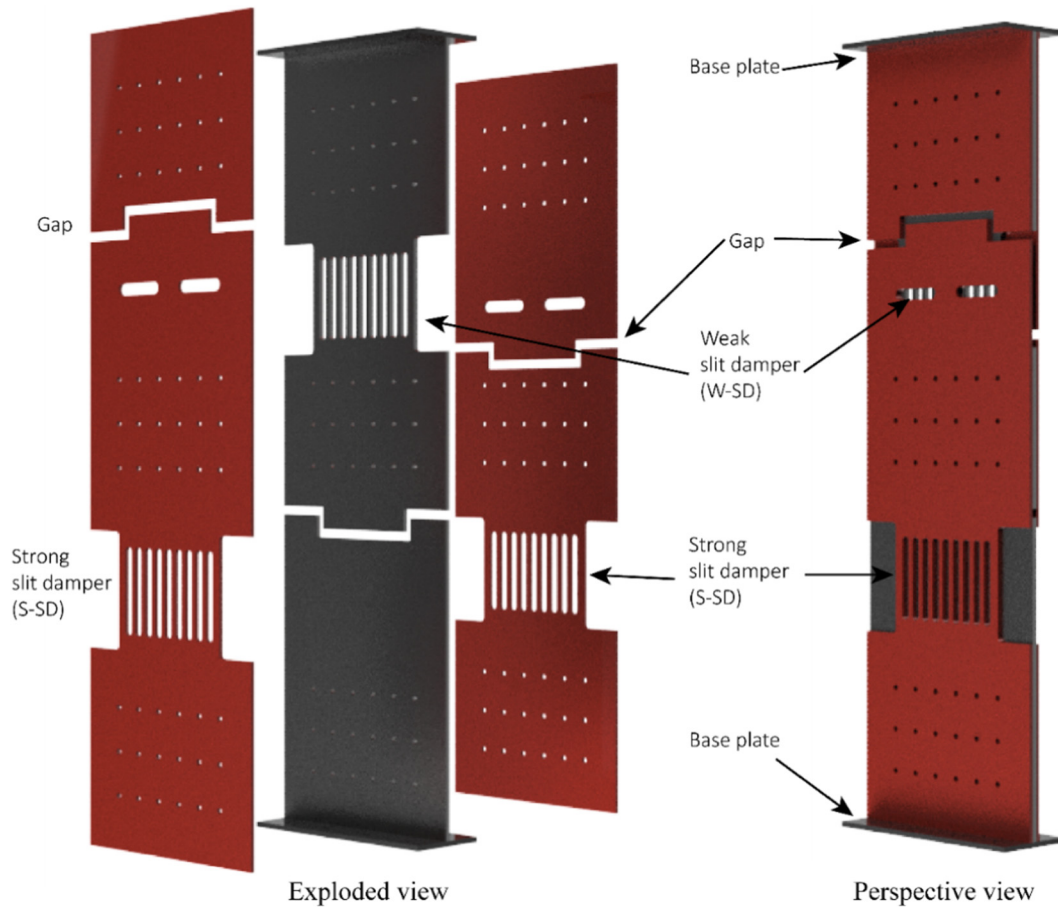


Fig. 1. Exploded view of the multi-slit damper.

damper reaches near the fracture point, further displacement is prevented by a stopper and the force is transferred to the strong slit damper. A simplified analytical model of the proposed damping devices is developed, verified, and calibrated by cyclic loading test and detailed finite element analysis in the ANSYS workbench. The applicability and effectiveness of the proposed damper are investigated by comparing the seismic performance of a 5-story RC ordinary moment frame before and after retrofit.

2. Design of a multi-slit damper

The multi-slit damper developed in this study is composed of three story-high steel plates combined together using high-strength bolts as shown in Fig. 1. The center plate with the weak slit damper is sandwiched between the two side plates with strong slit damper. The three steel plates are connected to each other by bolts at upper, middle, and lower parts, and only the center plate is fixed to the beams of the loading frame at the top and bottom. Each side plate is divided into the upper and lower part by the II-shaped gap which is used as a stopper to deactivate the weak slit damper located in the center plate and as a load transmitter to activate the two strong slit dampers in the side plates when a certain displacement is reached. As the lateral displacement further increases, even the gap in the center plate is closed and the strong slit dampers are also deactivated to prevent fracture. At this stage, the MSD works like a steel plate shear wall.

Typical steel plate slit damper is composed of many vertical strips as shown in Fig. 2. The in-plane stiffness of the slit damper subjected to horizontal shear force can be obtained based on the assumption that the ends of the narrow strips are fully restrained from rotation. The stiffness K_d , plastic moment M_p , yield force P_y , and yield displacement Δ_y of slit

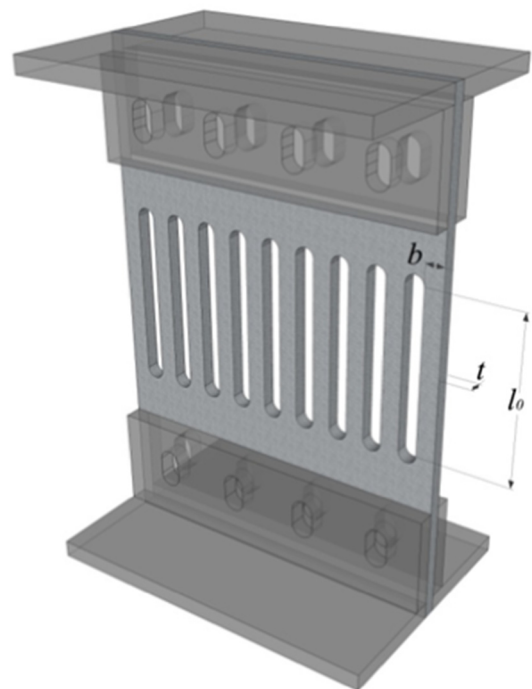


Fig. 2. Configuration of a typical steel plate slit damper.

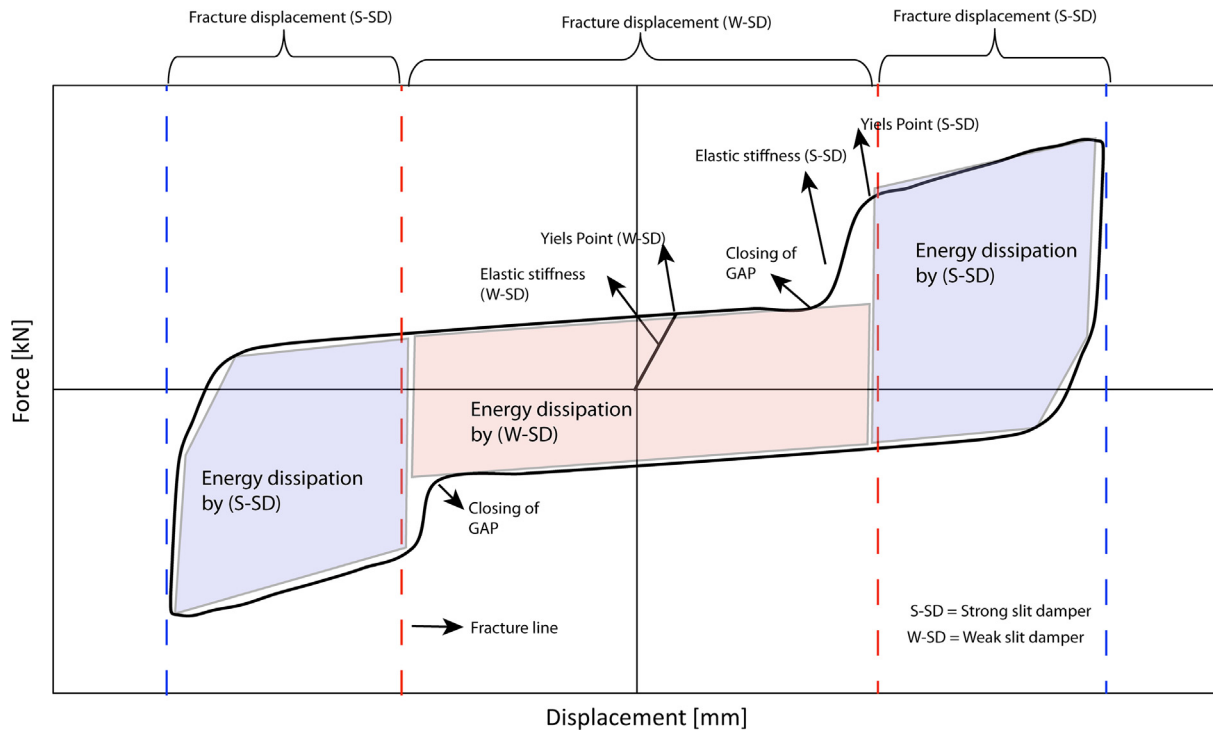


Fig. 3. Hysteresis curve of the multi-slit damper.

dampers are calculated as:

$$K_d = n \frac{12EI}{l_o^3} = n \frac{Etb^3}{l_o^3} \quad (1)$$

$$M_p = \sigma_y \frac{tb^2}{4} \quad (2)$$

$$P_{y,slit} = \frac{2nM_p}{l_o} = \frac{n\sigma_y tb^2}{2l_o} \quad (3)$$

$$\Delta_y = \frac{\sigma_y l_o^2}{Et} \quad (4)$$

where n is the number of strips, t is the thickness, b is the width, and l_o is the length of the vertical strip. More information on the behavior of a slit damper is presented in Chan and Albermani [4]. The MSD proposed in this study is composed of a weak and strong slit dampers connected in series, and the stiffness of the MSD can be calculated as follows:

$$K_{MSD} = \frac{K_{S-SD} \cdot K_{W-SD}}{K_{S-SD} + K_{W-SD}} \quad (5)$$

Based on the stiffness of the combined mechanism of the MSD, typical hysteresis curve of the MSD with two distinct yield points is shown in Fig. 3.

3. Cyclic loading test and validation by finite element analysis

This section presents the results of static loading tests performed on the full-scale prototype multi-slit damper (MSD). The purpose of the test is to assess the global response of the MSD and to establish its analysis model. The displacement controlled loading test was carried out on the prototype damper because the MSD is basically a displacement-dependent device which dissipates seismic energy by yielding of the steel strips. The stress-strain behavior of the steel material was obtained by the coupon test of the three hourglass-type specimens with a gauge length of 100 mm, and the average of the stress-strain relationship of the three specimens is presented in Fig. 4. Based on the coupon test results, the yield stress of the steel used in this study is

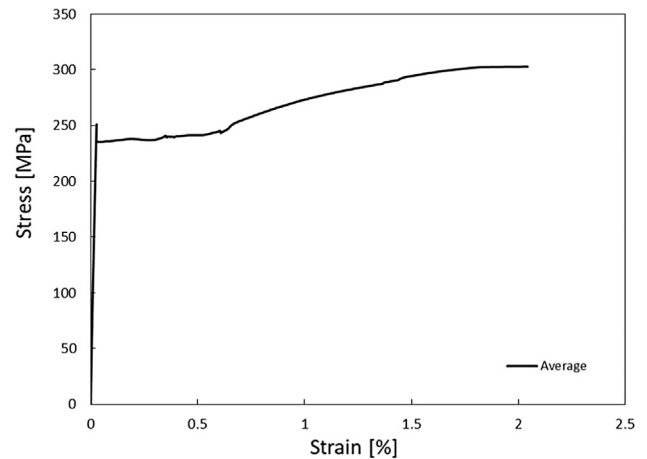


Fig. 4. Stress-strain relationship of coupons.

taken as 242 MPa.

3.1. Design-strength and dimensions of the MSD test specimen

The prototype multi-slit damper consists of three steel plates with the height of the test frame (2,913 mm) as shown in Fig. 5. Each steel plate is separated vertically by a 30 mm gap. The weak slit damper is located at the upper part of the center plate and two strong slit dampers are located at the lower part of the two side plates. It is designed to have the initial yield strength of 50 kN (weak slit part) at 5.3 mm lateral displacement and the second yield point of 122 kN (strong slit part) at 35 mm displacement. The thickness of the center plate is 20 mm and the thickness of the side plates is 15 mm. The lengths of the slit columns in the weak and the strong slit dampers are 270 mm and 230 mm, respectively. The complete dimensions and details of the MSD are presented in Fig. 5.

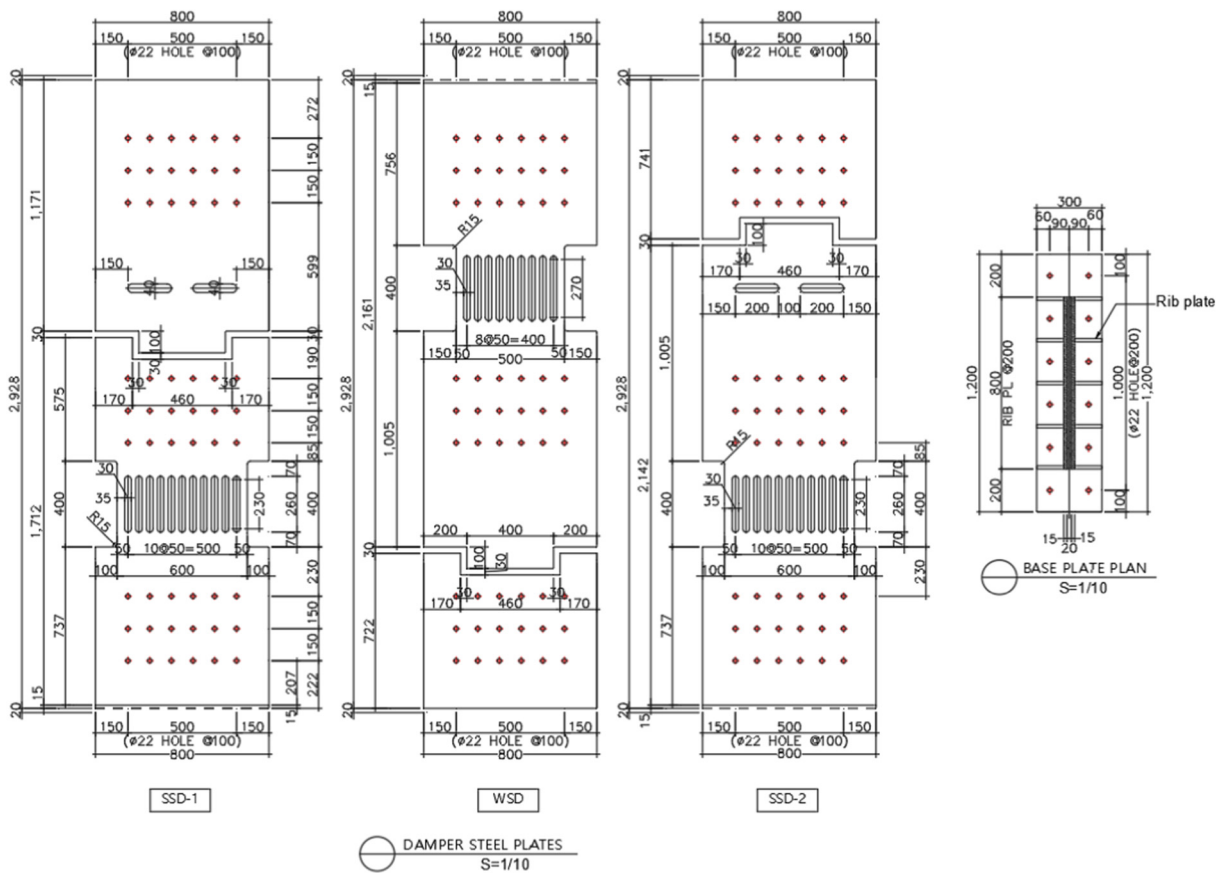


Fig. 5. Dimensions of the prototype multi-slit damper.

3.2. Experimental setup

To investigate the hysteretic behavior of the proposed damper, displacement-controlled cyclic loading test of the MSD was carried out using 1,000 kN hydraulic servo actuator. The MSD was installed in the steel frame with the pinned joints at the top and bottom of the columns for test. The height and span of the steel frame are 3,200 mm and 4,400 mm, respectively, as shown in the test setup (Fig. 6).

The loading protocol for the quasi-static cyclic displacement test, shown in Fig. 7, was applied as recommended in the ASCE 41-13 [14]. The test started with the displacement of 11.25 mm which corresponds to 0.25% of the target performance point for the life safety limit state (1.5% of the story height which is 3000 mm). After ten cycles of loading at 0.375% of the story height, the displacement is increased to 0.75% for the next five cycles. Then three cycles of the test were performed at each of the displacement of 1.5%, 2.0%, 3.0%, 4%, and 6% each of the story height.

The response of the loading test was monitored through a network of instrumentation including 22 strain gages attached on the surface of the strips of the slit dampers and near the gap, and three LVDT (linear variable differential transformer) were installed to measure the horizontal displacement at the top of the frame and the upper and lower parts of the MSD. Fig. 8 shows the locations of the strain gages attached on both sides of the MSD specimen.

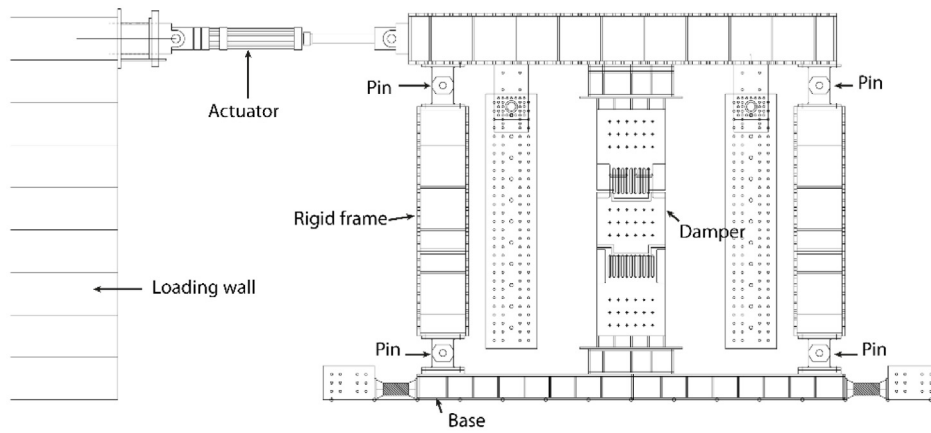
3.3. Cyclic loading test results

The hysteretic damper developed in this study consists of slit dampers with two different capacities to effectively resist both medium and strong earthquakes. The details of the cyclic load test are summarized in Table 1.

Fig. 9 shows the force-displacement relationship of the test

specimen obtained from the cyclic loading test. The weak slit damper yield first while the strong slit dampers remain elastic. Once the displacement of the weak slit damper reaches 30 mm, which is slightly smaller than the fracture displacement, the gaps between the top and bottom side plates are closed, and the load is transferred to the strong slit dampers at the bottom side plates while the weak slit damper is prevented from further deformation. In this way, the slit dampers are prevented from being fractured and remain functional throughout earthquake excitations. It is observed that the weak slit part yield first at the displacement of 5.3 mm and the load increases again until the strong slit parts yield at the displacement of 38 mm. Fig. 9 also shows that the dissipated energy, which is the area included in the hysteresis curve, increases with the increase in the displacement because both slit dampers are activated. The hysteresis curves are nearly symmetrical in both directions. The first yield force of the weak slit damper is 50 kN which is the same with the theoretical yield point computed using Eq. (3). The second yield force of the strong slit damper, however, is approximately 160 kN while the theoretical value is 130 kN. This may be due to the participation of a tension field across the steel plates at large displacement. The higher post-yield stiffness of the strong slit damper than that of the weak slit damper can be contributed to the same reason.

It was observed during the first cycle of 1.5% drift that the side plate gaps were closed at the displacement of 30 mm, but due to reasons such as slip of bolted connections, local deformation, and slight twist of the steel plates during the previous loading steps, the gap was closed at larger displacement in the subsequent cycles. Similarly, at the final stages of the test, the center plate gap was closed at the displacement of 80 mm increased from the initial value of 60 mm. At the displacement larger than 60 ~ 80 mm the load increased significantly due to the fact that the deformation of all slit dampers was stopped by the closing of all gaps and the steel plates acted like a steel plate shear wall.



(a) Overall configuration the test setup



(b) Photograph of the test setup

Fig. 6. Test setup for cyclic loading test of the MSD.

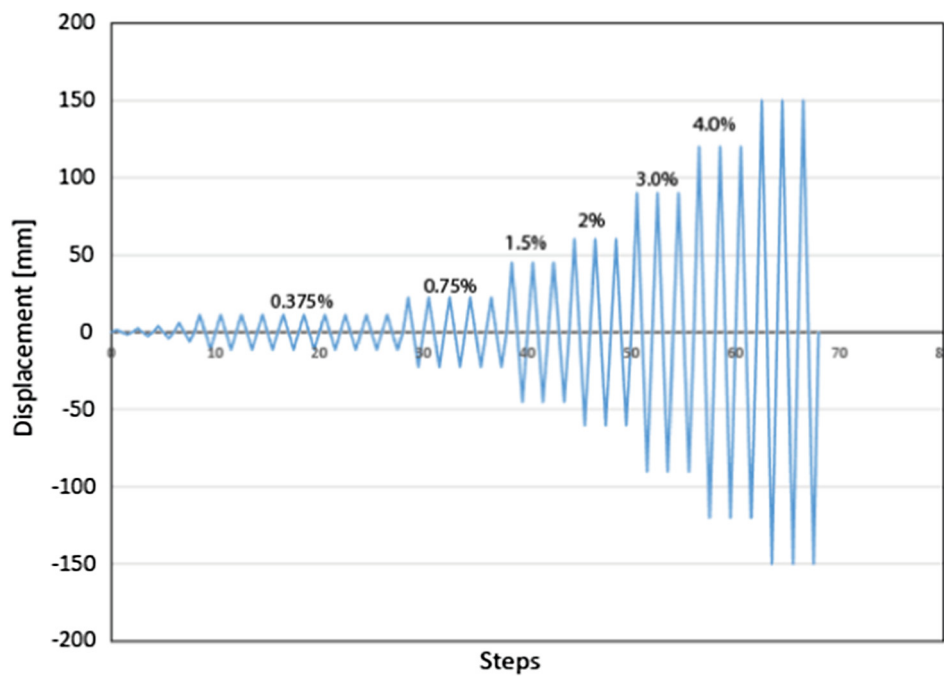


Fig. 7. Loading protocol used in the cyclic test.

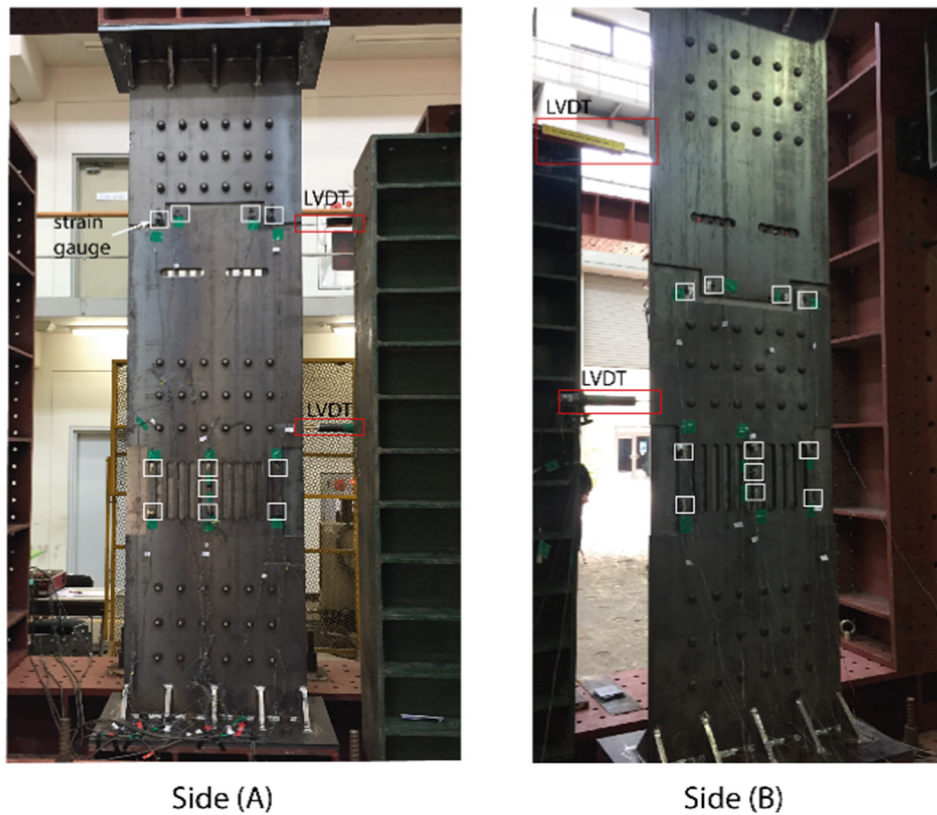


Fig. 8. Locations of strain gauges and LVDTs for loading test.

The closing of the gap and contact between the lower and upper steel plates at the 1.5% drift is shown in Fig. 10(a), and the local deformation or distortion around the gaps at 3% drift is depicted in Fig. 10(b). Due to the local deformation around the gap caused by the large stress concentration at the contact area, the yield displacement changed at each loading cycle. At the loading cycle corresponding to 6% of the story height, the load transfer between the upper and lower steel plates was terminated when the relative out-of-plane deformation of the upper and lower plates became larger than the thickness of the plates. Fig. 11 shows the out-of-plane movement between the upper and lower plates and the permanent deformation of the slit part at failure.

The strain records measured by the strain gauge attached at the center of the strong slit damper is shown in Fig. 12. It can be observed in Fig. 12(a) that the strong slit damper was within the elastic range before the displacement reached 30 mm which is the gap distance. Once the displacement exceeded 38 mm the strong slit damper yielded and the strain increased until the center plate gap was closed and the yielding of the strong slit damper stopped at the displacement of around 90 mm in one side. In the other side the strain kept increasing until the displacement reached 120 mm due to the local deformation around the center plate gap. From the recording of the strain gage, it can be

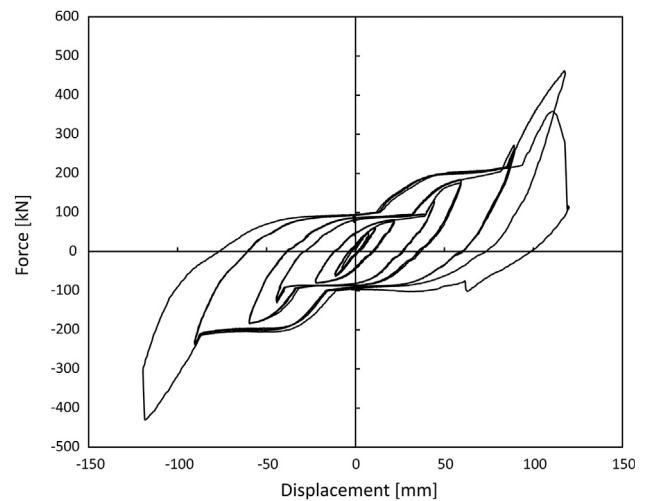


Fig. 9. Hysteresis of multislit damper obtained from the loading test.

Table 1
Details of the cyclic loading test.

Drift rate (%)	Target displacement mm	Cumulative displacement mm	No. of cycle #	Time sec/cy	Speed mm/sec	Frequency Hz/cy	Total time sec	Force at each cycle kN
0.25	7.5	30	2	60	0.50	0.0167	120	48.63
0.375	11.25	45	10	90	0.50	0.0111	900	61.74
0.75	22.5	90	5	135	0.67	0.0074	675	73.65
1.5	45	180	3	270	0.67	0.0037	810	129.10
2	60	240	3	360	0.67	0.0028	1,080	182.81
3	90	360	3	432	0.83	0.0023	1,296	236.20
4	120	480	1	576	0.83	0.0017	1,728	430.50

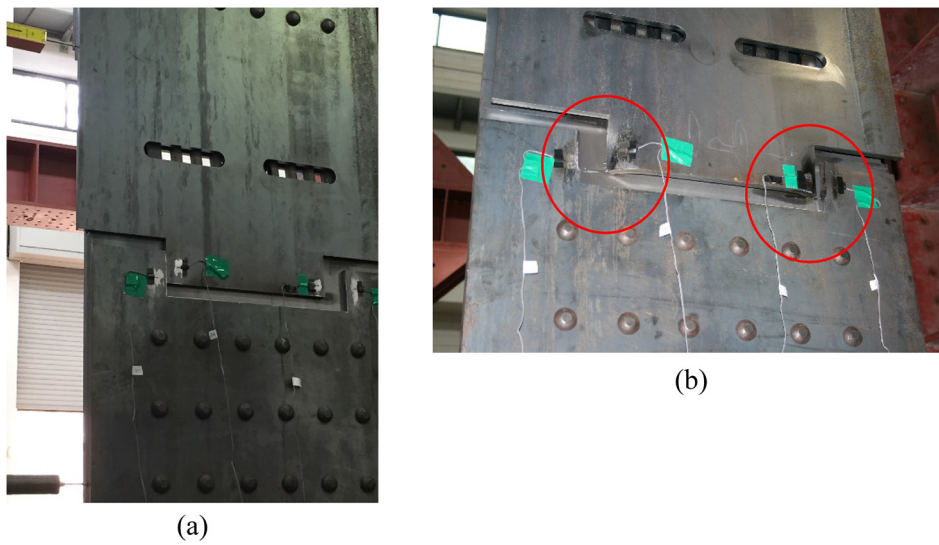


Fig. 10. Deformation of the test specimen: (a) Closing of the gap; (b) local deformation around the gaps at 3% drift.

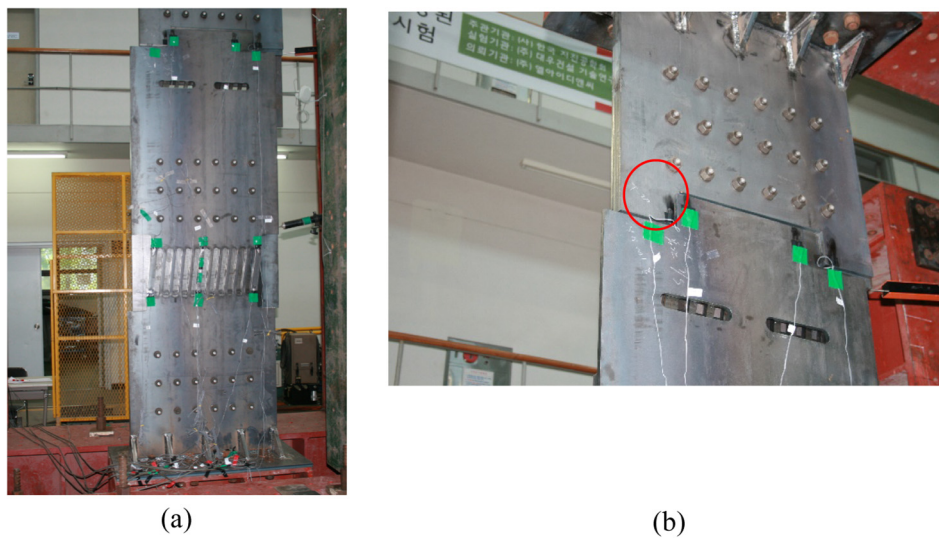


Fig. 11. Failure state of the specimen: (a) Permanent deformation at the slit part; (b) out-of-plane movement of the upper and lower plates.

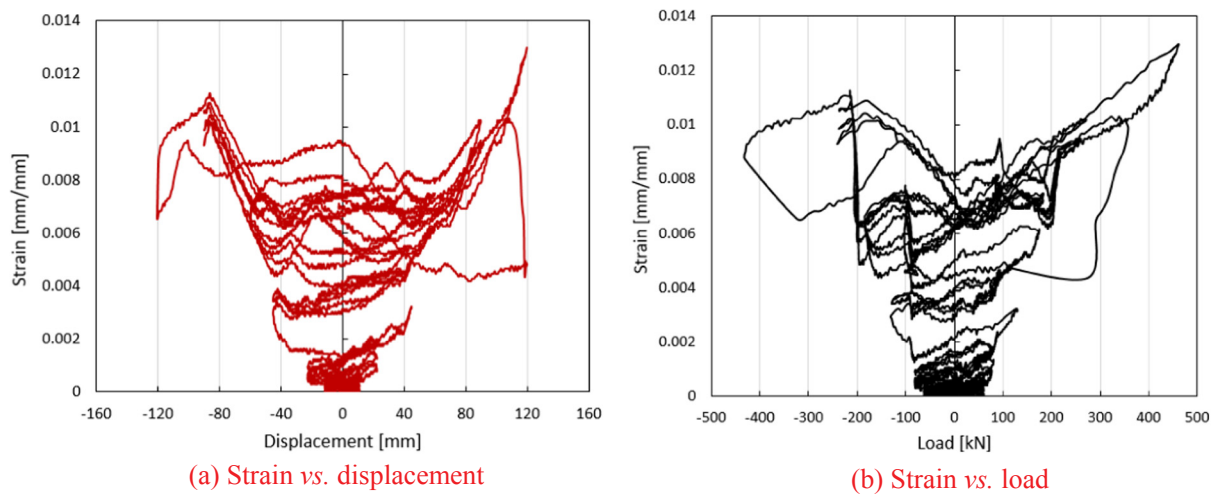


Fig. 12. Recording of a strain gage attached to one of the steel strips in the strong slit damper.

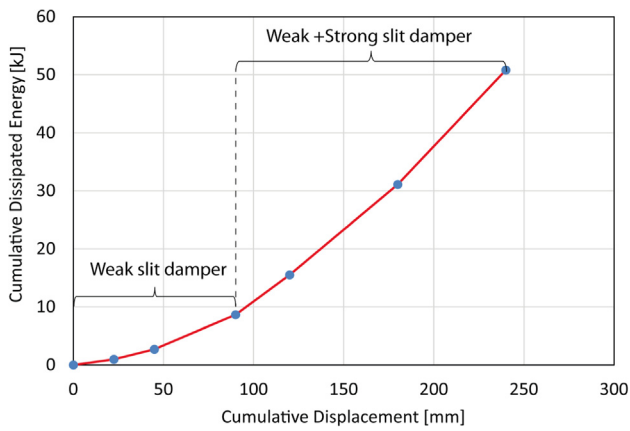


Fig. 13. Accumulated energy dissipation obtained from the cyclic loading test of MSD.

observed that significant deformation occurs in the slit damper, dissipating large amount of energy.

Based on the test results, the effective viscous damping ratio of the multi-slit damper, ζ_{eff} , can be estimated using the following equation [15]:

$$\zeta_{eff} = \frac{1}{4\pi} \cdot \frac{E_D}{E_{S0}} \tag{6}$$

where E_{S0} is the potential energy stored at the maximum displacement δ_{max} , and E_D is the dissipated energy during one cycle of vibration. E_{S0} is obtained by $1/2 \cdot k_{eff} \cdot \delta_{max}$, where k_{eff} is the effective stiffness at the

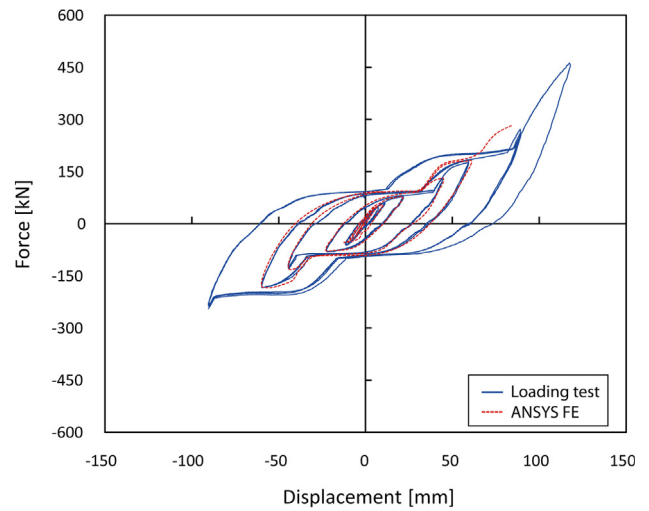


Fig. 15. Comparison of hysteresis curves of MSD obtained from cyclic loading test and FE analysis.

maximum displacement, and E_D is the area of the hysteresis curve. The forces at the maximum displacements of each loading cycle were observed to be identical in both the loading directions. The dissipated energy per cycle at the target displacement of ± 60 mm (at 2% drift) was computed to be 15,500 kN-mm. The cumulative dissipated energy versus the cumulative displacement curve from the experiment is depicted in Fig. 13. The growth rate of the cumulative dissipated energy increases significantly when both the weak and the strong slit dampers

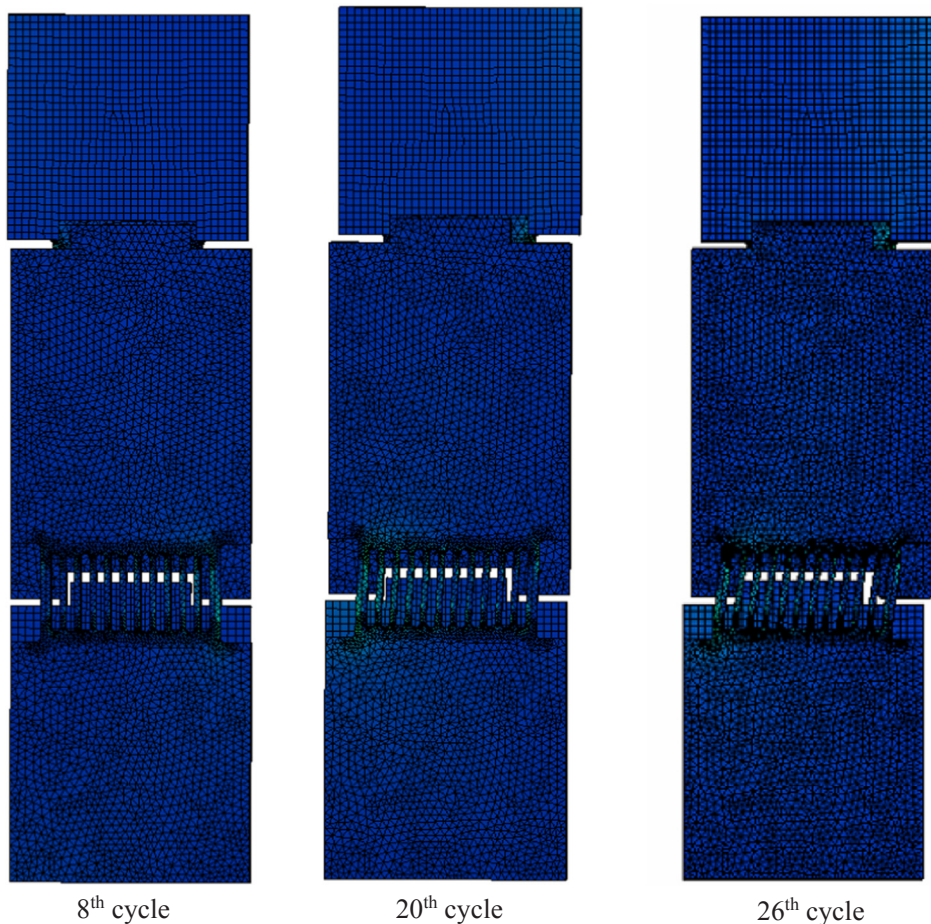


Fig. 14. Stress distribution in MSD obtained from ANSYS finite element analysis.

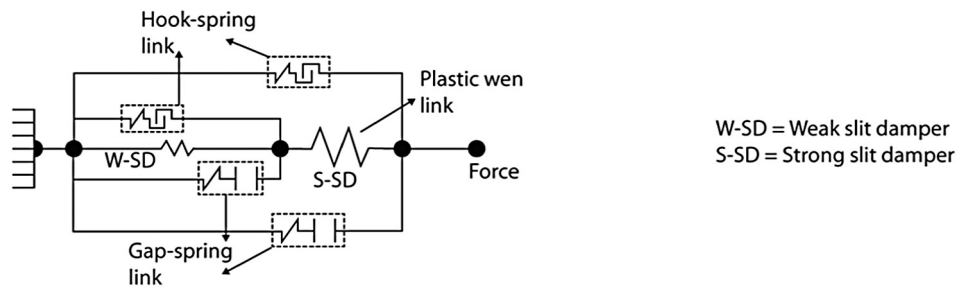


Fig. 16. Analysis model for the multi-slit damper.

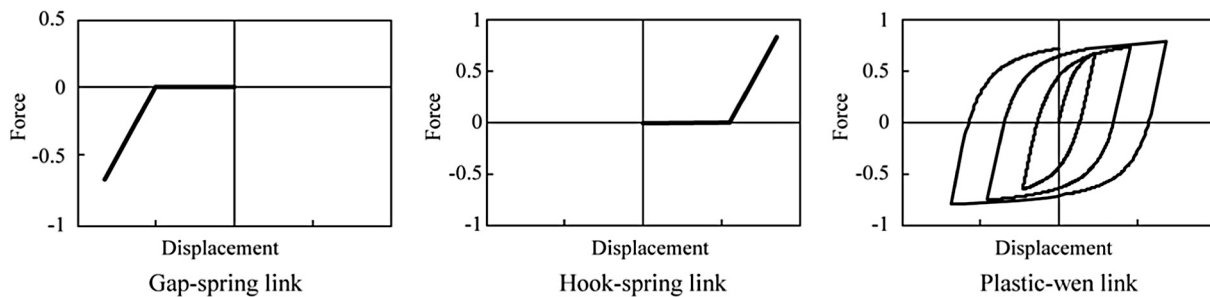


Fig. 17. Force-displacement relationships of the link elements used in the analysis model.

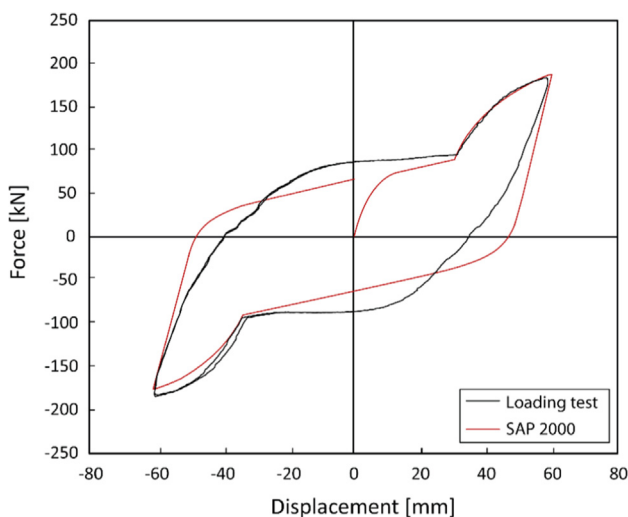


Fig. 18. Hysteresis curves of the multi-slit damper obtained from experiment and SAP2000 analytical model.

are activated.

3.4. Finite element analysis results

To validate the cyclic loading test results, finite element analysis of the test specimen was carried out using the ANSYS [16]. The steel plates were modeled by the 8-node hexahedron solid element with an average element size of 10 mm. The stress contours in the damper at the 8th, 20th and 24th cycle obtained from the FE analysis are shown in Fig. 14. The figure shows that the stress concentration occurs at the slit part and at the contact of the two plates. The other parts remain elastic during the loading stage. The comparison of the hysteresis curves at 2% interstory drift obtained from the FE analysis and the loading test are in good agreement as shown in Fig. 15. As the lateral displacement increases the match between the two results gradually deviates from each other due to various reasons such as local damage around the gap, a twist of the steel plate, a slip of the bolted connections, etc.

4. Analysis model of the multi-slit damper

In this section, the force-displacement relationship of the multi-slit damper was developed for the general purpose structural analysis software SAP 2000 [17] using various link elements. The nonlinear relationship of the damper unit obtained from the test was idealized as the curvilinear curve in such a way that the areas under the actual and the idealized curves are the same.

The damper was analytically modeled by combining three types of nonlinear links such as HOOK-SPRING, GAP-SPRING, and WEN PLASTIC links as shown in Fig. 16. The force-displacement behavior of each link is presented in Fig. 17. The model consists of two WEN PLASTIC links connected in series representing the weak slit damper (W-SD) and the strong slit damper (S-SD). These links account for the stiffness and energy dissipation of the slit dampers. The nonlinear HOOK-SPRING element accounts for the gap in tension, and the GAP-SPRING link limits the slit dampers to work in a stroke range in compression. The force-displacement relationship of the multi-slit damper obtained from the loading test at a displacement of 60 mm is shown in superposition with the corresponding cycle derived from the numerical simulation in Fig. 18, which demonstrates that the behavior of the multi-slit damper can be properly predicted with the analytical model within the test range. Even though there is a slight mismatch between the test data and analysis model, it will not affect the structural response significantly because the analysis model is developed in such a way that the areas of the hysteresis curves obtained from the test and the analysis model are almost the same.

5. Seismic retrofit of a structure with MSD

5.1. Design of analysis model structure

In this section, the seismic performance of a reinforced concrete (RC) structure retrofitted with the MSD was evaluated using the analysis model developed above, and the results were compared with those obtained from analysis of the structure retrofitted with conventional slit dampers in terms of energy dissipation and load resisting capacity under strong earthquakes. The analysis model structure depicted in Fig. 19 is a 5-story RC moment frame designed only for gravity and wind load.

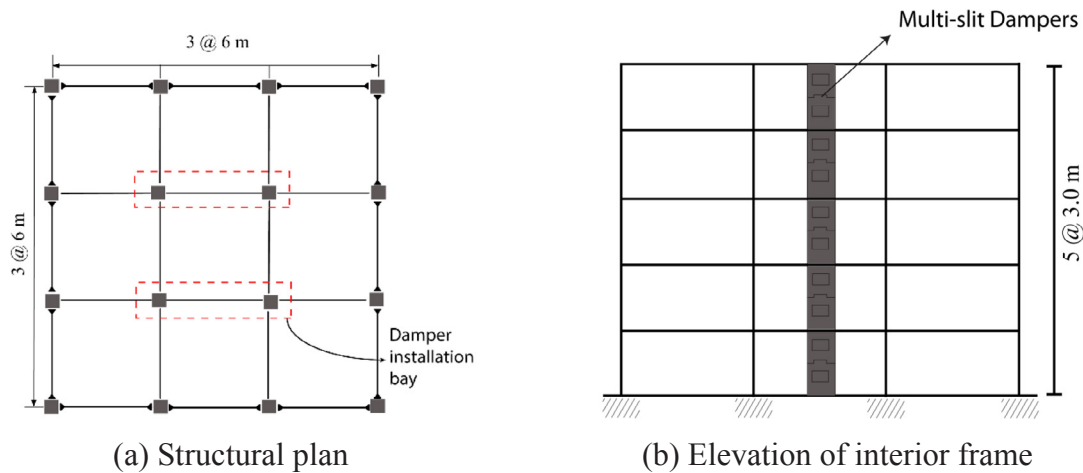


Fig. 19. 5-story RC analysis model structure.

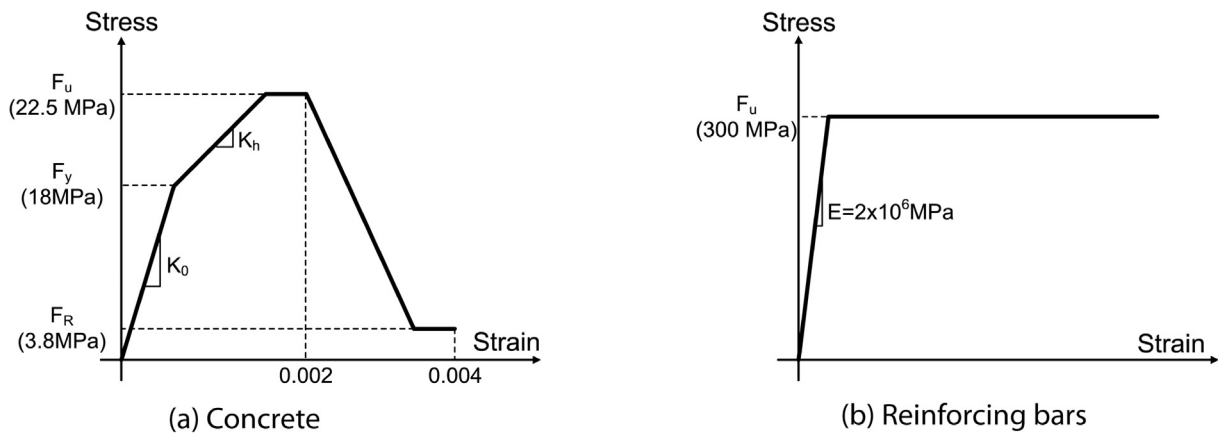


Fig. 20. Nonlinear stress-strain relationship of structural materials.

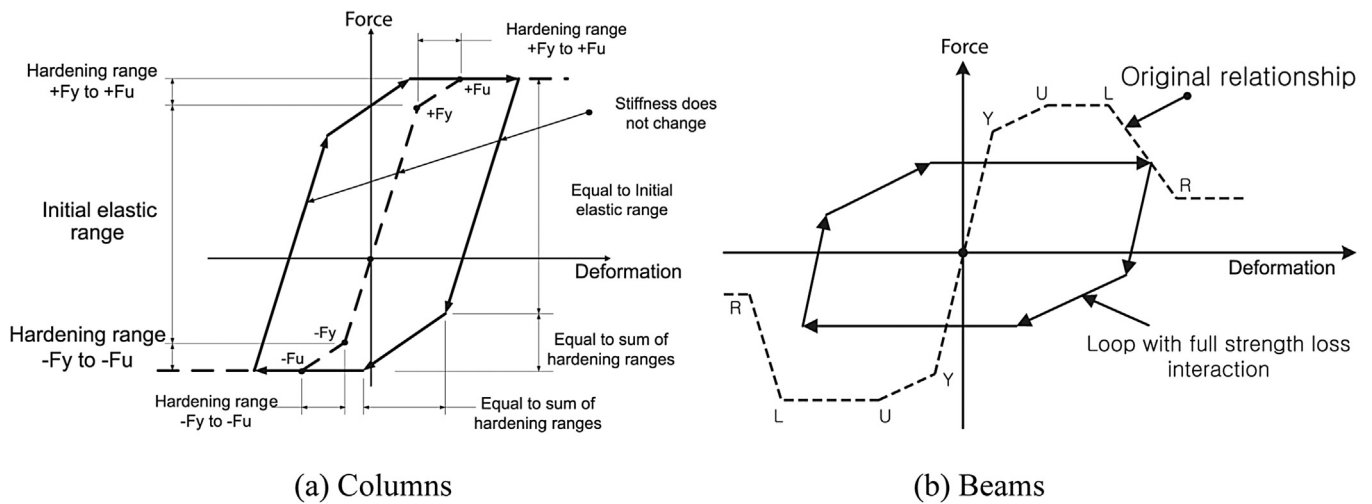


Fig. 21. Hysteresis loops of RC beams and columns (ASCE/SEI 41-13).

The multi-slit dampers were installed in the center bays of the interior frames as shown in Fig. 19. For comparison purpose, the same analysis model structure retrofitted with the conventional slit dampers were also analyzed. The dead and live loads used in the structural design are 5 kN/m² and 2.5 kN/m², respectively, and the wind load was estimated using the basic wind speed of 30 m/s. The ultimate strength of concrete is 22.5 MPa at the strain of 0.002, and the residual strength is defined as 17% of the ultimate strength as shown in Fig. 20(a). The

reinforcing steel bars were modeled with bi-linear lines with a yield strength of 300 MPa as presented in Fig. 20(b).

The fundamental natural period of the model structure is 0.48 s and a fundamental modal damping ratio of 5% of critical damping was used in the analyses. The material nonlinearity was accounted for by defining localized plastic hinges at the ends of structural elements. Bending members are composed of two end rotation type moment hinges defined according to the ASCE/SEI 41-13 [14] as shown in

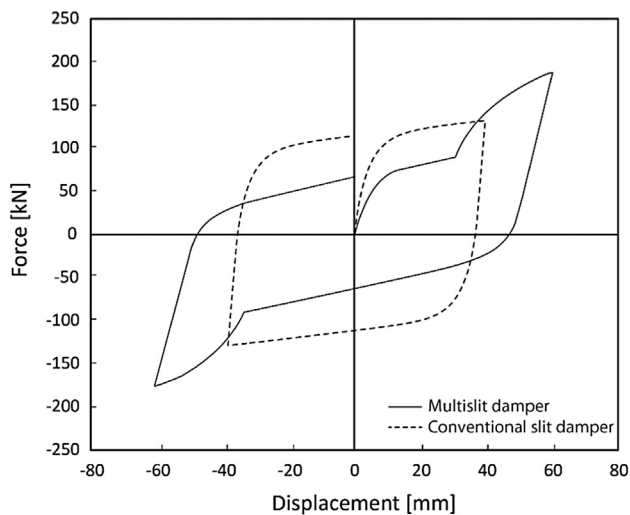


Fig. 22. Hysteresis curves of the MSD and conventional slit damper designed to have the same energy dissipation capacity.

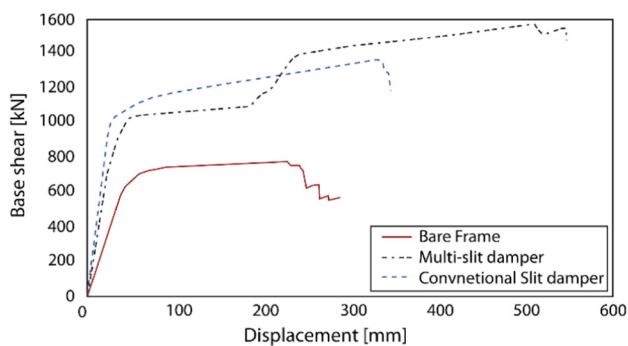


Fig. 23. Pushover curves of the model structure before and after seismic retrofit.

Table 2
Earthquake records used for dynamic analysis.

ID No.	Record No.	Earthquake name	Component	PGA Max. (g)
1	68	San Fernando	SFERN/PEL180	0.23
2	174	Imperial Valley	IMPVALL/H-EII230	0.39
3	721	Superstition hills	SUPERST/B-ICC000	0.36
4	752	Loma Prieta	LOMAP/CAP000	0.53
5	953	Northridge	NORTHR/MUL009	0.52
6	1111	Kobe Japan	KOBE/MIS000	0.51
7	1485	Chi-Chi	CHICHI/CHY101-E	0.44

Fig. 21. In consideration of cracked sections, the flexural stiffness and shear stiffness of the beams was reduced to 50% and 40% of the uncracked values, respectively. For the columns, flexural stiffness was reduced by 50% to 70% depending on the level of axial load, and the shear stiffness was reduced to 40% of the original value.

The displacement-dependent dampers such as metallic dampers and friction devices are relatively cheap, durable, and generally show well-defined hysteretic behavior; therefore primary structural members can be safely designed using capacity spectrum procedures. In this paper, the capacity spectrum method presented in ATC-40 [18] was used to determine the required added damping to satisfy the given performance limit state. FEMA 273 [19] also contains provisions for the design of structures with passive energy dissipation systems.

The conventional slit dampers used for comparison purpose has the configuration of a typical slit damper shown in Fig. 2, which was assumed to be installed between upper and lower beams using rigid

trusses [20]. Total of 25 strips exist in the conventional slit damper with the steel strip length l_0 of 250 mm, strip width b of 20 mm, and thickness t of 20 mm. The conventional dampers have single slit part as compared to the MSD developed in this study. The conventional slit dampers were designed to have the same energy dissipation capacity with the MSD when they deform to their limit states as shown in Fig. 22. The conventional steel slit dampers have 6% higher initial stiffness than the MSD but have smaller fracture displacement of 38 mm.

In this study two level seismic performance objectives were applied for retrofit design: which is to limit the maximum inter-story drift ratio (MIDR) within 1.5% of the story height for design earthquakes (DE) (Life Safety limit state), and to limit the maximum inter-story drift ratio (MIDR) within 2.5% of the story height for maximum considered earthquakes (MCE) (Collapse Prevention limit state). It was observed that the model structure with two MSD at each story satisfied the two limit states.

5.2. Nonlinear static analysis results

The nonlinear static pushover analyses of the model structure with and without slit dampers were carried out using the lateral load proportional to the fundamental mode shape. Fig. 23 shows the pushover curves of the model structure before and after the retrofit. It can be observed that the stiffness and the strength of the model structure increase significantly as a result of the seismic retrofit. As the weak and strong slit dampers are connected in series, the stiffness of the MSD is smaller than that of the conventional damper. Consequently, the initial stiffness of the structure retrofitted with the MSD turned out to be smaller than that of the structure retrofitted with the conventional slit dampers. However, the ductility of the structure retrofitted with the conventional dampers is smaller than that of the structure retrofitted with MSD because the conventional slit dampers fracture at the displacement of 38 mm, whereas fracture of the MSD is prevented by stopping mechanism.

5.3. Nonlinear dynamic analysis results

To validate the efficiency of the proposed MSD and conventional slit dampers for mitigation of the seismic response, nonlinear dynamic time history analyses were carried out using seven earthquake records obtained from the PEER NGA database [21]. The earthquake records used for the analysis are shown in Table 2. The selected ground motion records were from large magnitude events recorded at moderate fault-rupture distances on stiff soil or rock sites. The model structure was assumed to be located in the south of Los Angeles (34°N, 118.2°W), at which the spectral acceleration parameters at the short period (S_{DS}) and at 1 s (S_{D1}) are 1.4 and 0.7, respectively, according to ASCE 7-13 [19] as shown in Fig. 24(a). Similarly, MCE level design spectrum shown in Fig. 24(b) has the spectral acceleration parameters of S_{DS} and S_{D1} equal to 2.1 and 1.05, respectively.

Nonlinear time-history analyses of the model structure were carried out using the 7 sets of scaled ground acceleration records. The earthquake records were scaled to the design earthquake (DE) spectrum and the maximum considered earthquake (MCE) spectrum as presented in Fig. 23. They were scaled in such a way that in the period range from $0.2T$ to $1.5T$, where T is the fundamental period, the average of the SRSS (square root of sum of square) spectra from all acceleration history pairs does not fall below 71% of the corresponding ordinate of the target response spectrum as recommended in ASCE 7-13 [22]. The engineering demand parameters for evaluating the seismic performance are the maximum inter-story drift ratios (MIDR), the maximum roof displacements, and the energy dissipation in the model structure.

The roof displacement time histories of the model structure with and without the dampers are presented in Fig. 25 for the three selected earthquakes scaled to the DE and the MCE level target spectra. The

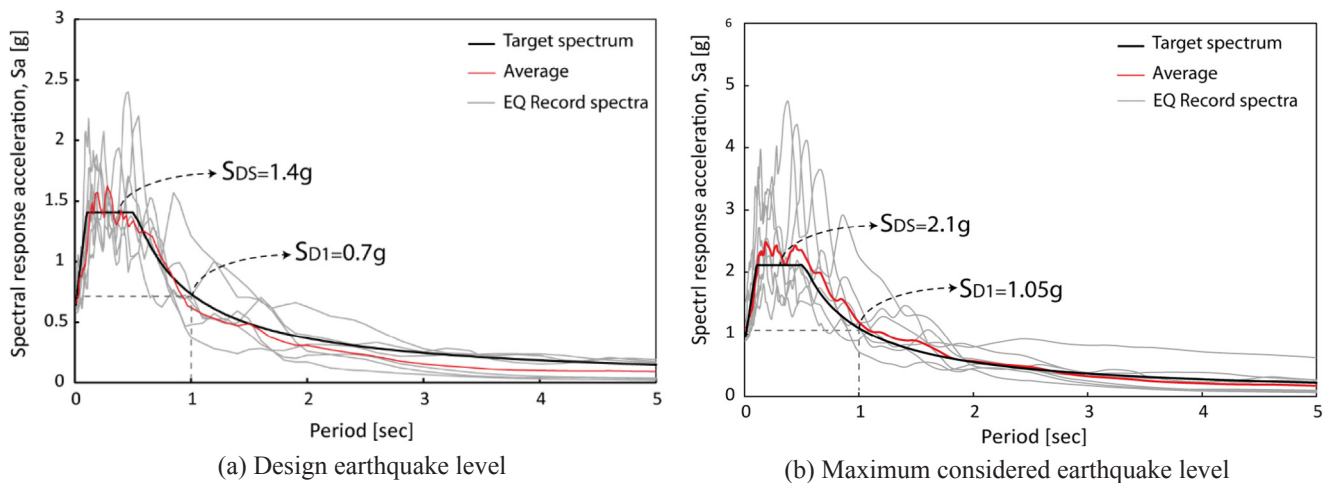


Fig. 24. Response spectra of the selected ground motions and the target spectra.

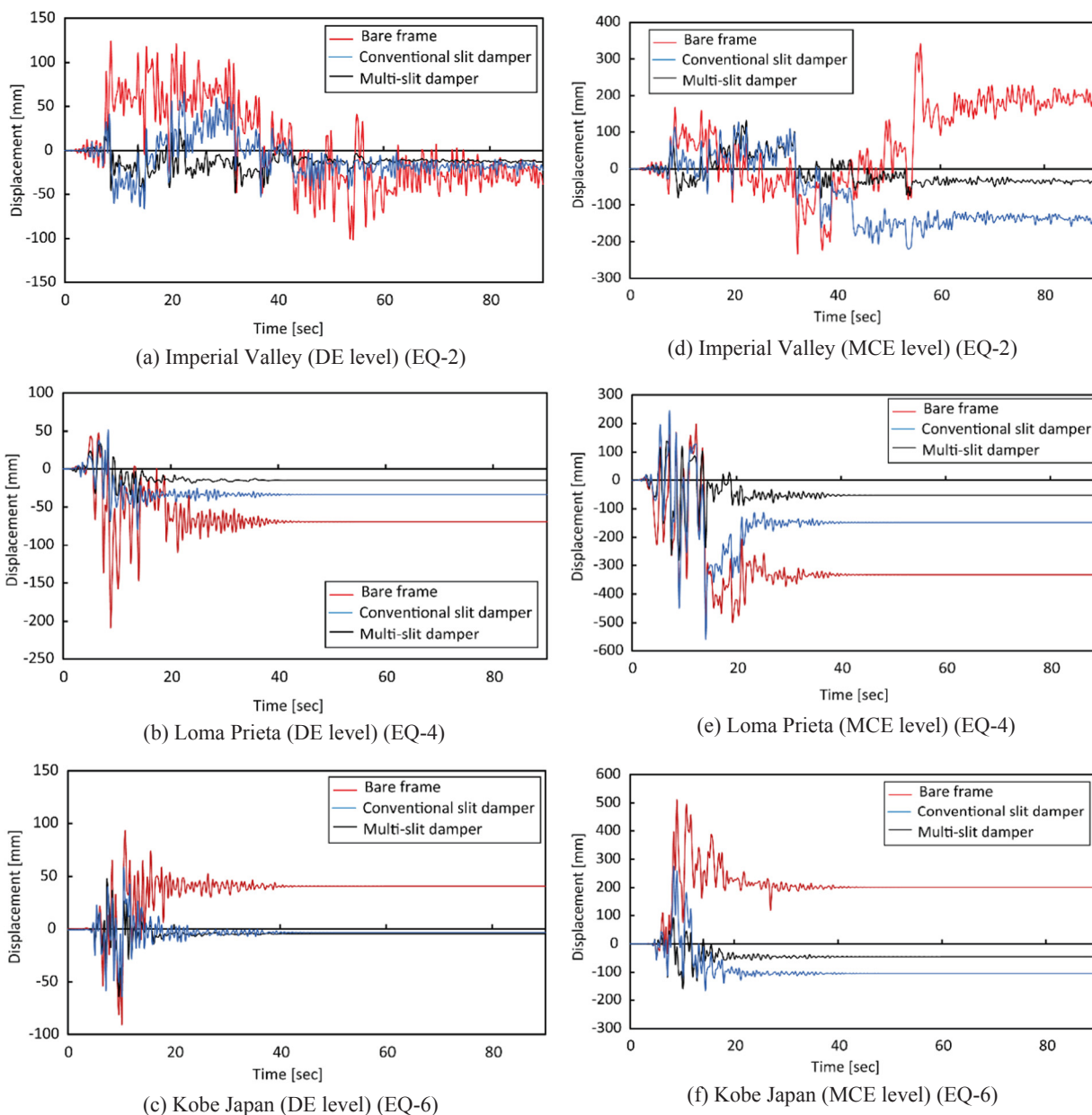


Fig. 25. Roof displacement time histories of the model structure with and without dampers.

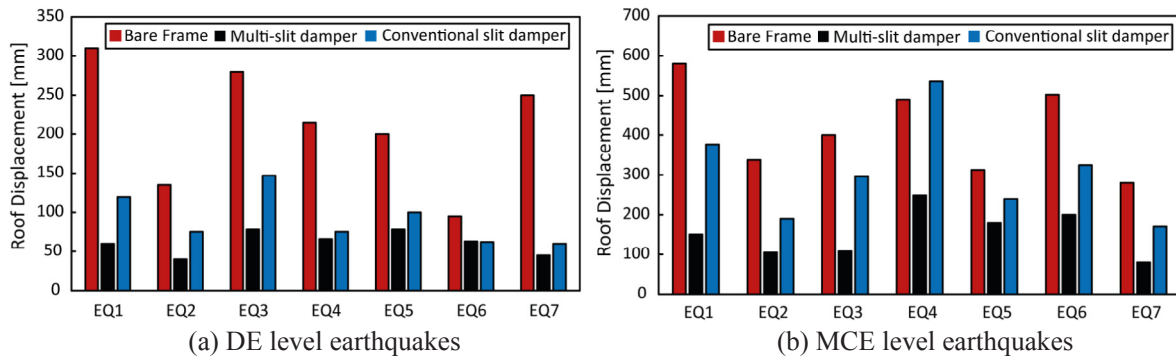


Fig. 26. Maximum roof displacement of the model structure with and without dampers.

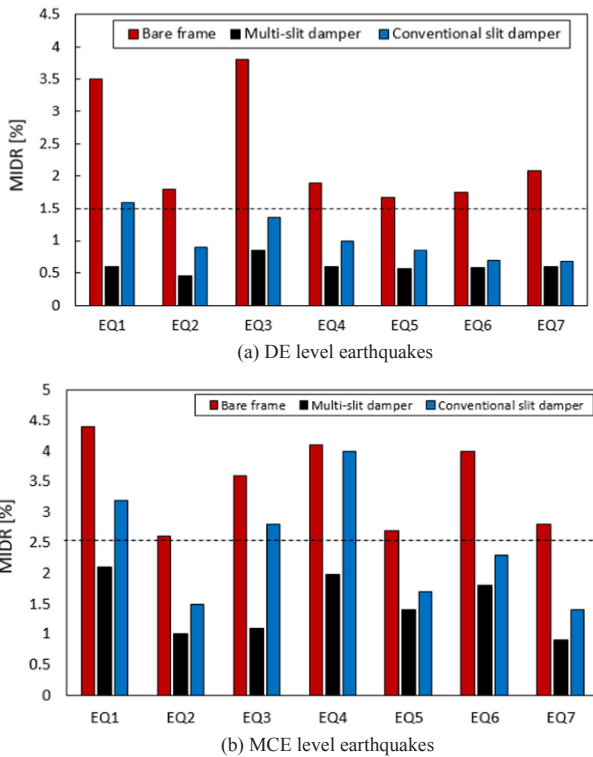


Fig. 27. Maximum inter-story drift ratios of the model structure with and without dampers subjected to DE and MCE level earthquakes.

figure shows that both the maximum roof displacement and the permanent residual lateral drift decrease after the dampers are installed. The large residual displacement remaining in the bare structure results from inelastic deformation of beams and columns. The reduction in the residual displacement in the structure retrofitted with the dampers implies that the damage in the main structural components is reduced. The reduction in the maximum roof displacement and the residual displacement is most significant in the structure retrofitted with the MSD subjected to the MCE level earthquakes. The maximum roof displacements of the model structure subjected to the seven earthquake records are plotted in Fig. 26. The maximum roof displacements of the model structure retrofitted with the MSD are smaller than those of the structure retrofitted with the conventional dampers by 38% for DEs and 46% for MCEs. This is due to the fact that in the structure retrofitted with the conventional slit dampers some slit dampers are fractured at large displacement and lose energy dissipation capability, while in the structure retrofitted with the MSD the dampers are prevented from fracture and function effectively throughout the earthquake excitations.

Fig. 27 depicts the maximum inter-story drift of the model structure

with and without dampers subjected to the seven earthquakes scaled to the DE and MCE level design spectra. It can be observed that the inter-story drift of the bare frame exceeds the limit state of 1.5% and 2.5% of the story height for all earthquakes scaled to the DE and MCE target spectra, respectively. In the structure retrofitted with the MSD, the inter-story drifts are reduced below the given limit states for all the earthquake records. However, the maximum inter-story drift exceeds the limit state for one and three earthquakes scaled to the DE and MCE spectra, respectively, in the structure retrofitted with the conventional slit dampers. It is observed that the mean inter-story drift of the structure retrofitted with MSD is 36% less than that of the structure retrofitted with the conventional dampers. Especially for MCE level EQ4 (Loma Prieta) earthquake, the maximum inter-story drift of the structure retrofitted with the conventional dampers is almost the same with that of the bare structure. In this case, the maximum inter-story drifts of some stories exceed the fracture point of the conventional slit dampers, resulting in loss of their stiffness and energy dissipation capacity.

The performances of the MSD and the conventional slit dampers were also compared in terms of inelastic energy dissipation under MCE level shaking in Fig. 28, which depicts the time history of the dissipated energy in the model structures subjected to the Imperial Valley earthquake scaled to the MCE level. It can be observed that in the bare structure 52% of the input seismic energy is dissipated by the inelastic deformation of the structural elements, and the remaining input energy is dissipated by the inherent modal damping. On the other hand, the significant amount of energy is dissipated due to the stable hysteretic behavior of the slit dampers in the retrofitted structures. It is observed that the MSD dissipate 81% of the total energy while the conventional slit dampers dissipate only 65% of the input energy due to fracture of some slit dampers.

6. Conclusions

This paper proposed a new steel slit damper composed of story-high steel plates with weak and strong slit parts connected in series. The weak slit damper part was designed to work during low to medium seismic excitation, while the strong slit part was designed to be activated at large earthquakes. The energy dissipation capability of the proposed damper was investigated by cyclic loading test and finite element analysis. The results of the experiment and FEM analysis were used to develop an analytical model for commercial structural analysis programs. The dampers were applied to seismic retrofit of a 5-story RC moment frame, and the structural responses were compared with those of the structure retrofitted with conventional slit dampers.

It was observed in the cyclic loading test of the multi-slit damper that two distinct yield points existed as designed and that the damper showed stable hysteretic behavior at the lateral displacement larger than 4% of the story height. The force-displacement relationship of the test specimen obtained from finite element analysis matched well with

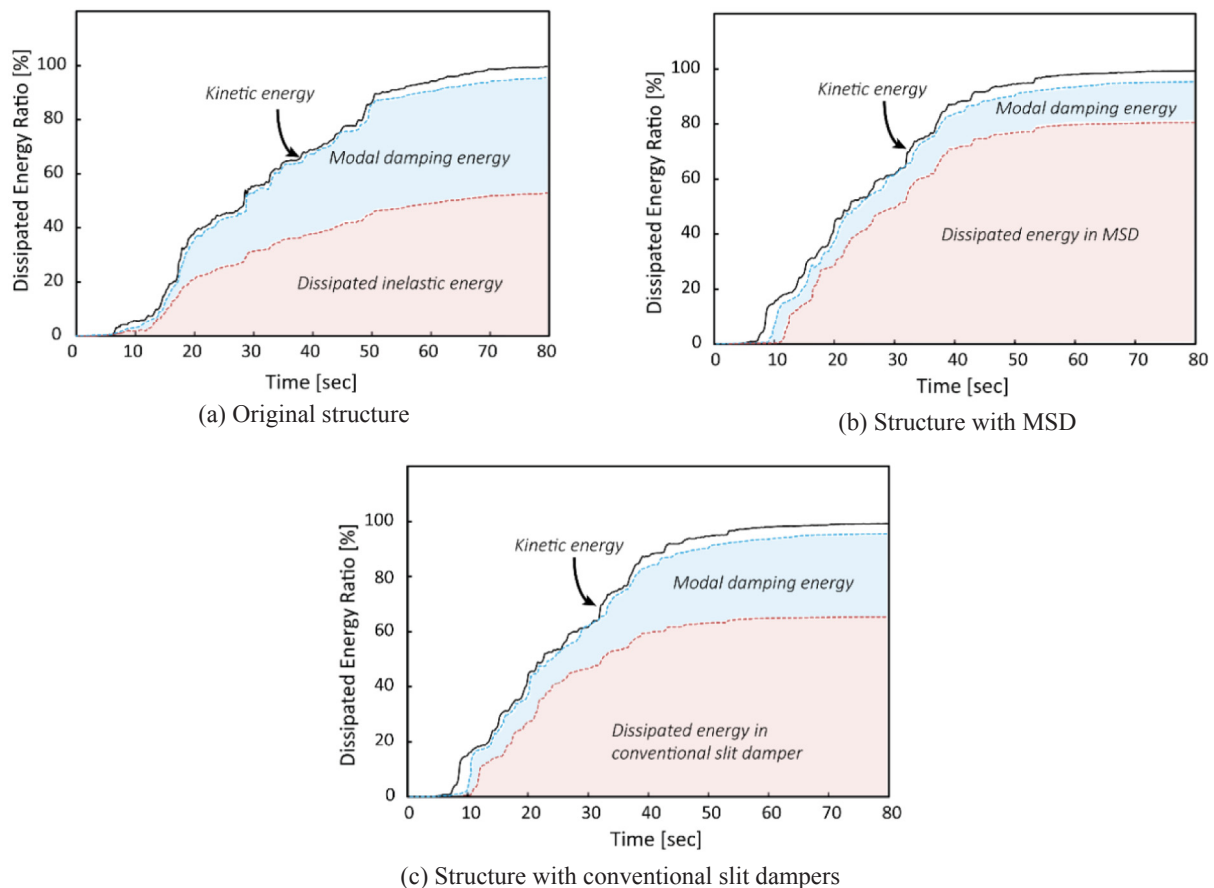


Fig. 28. Dissipated energy in the model structure subjected to the MCE level Imperial Valley earthquake.

the test results. The analysis model made by a combination of three nonlinear link elements turned out to simulate the test result quite well in a general purpose structural analysis software. The nonlinear static analysis of the 5-story model structure showed that the structure retrofitted with the proposed dampers had larger ductility capacity at collapse compared with the structure retrofitted with conventional slit dampers. The nonlinear dynamic analysis of the model structure showed that the mean inter-story drift and the mean maximum displacement of the retrofitted structure were respectively 36% and 47% smaller than those of the structure retrofitted with conventional slit dampers.

Based on the experimental and analysis results, it can be concluded that the MSD is an effective seismic protection system for framed structures. It should be pointed out, however, that there is a possibility of different out-of-plane displacement of the steel plates in MSD when the earthquake causes strong torsional response of structures. In a highly irregular structure with large torsional behavior, the thickness of the steel plates needs to be increased to prevent large out-of-plane deformation, and the dampers should be located in such a way that the stiffness eccentricity is removed and consequently the torsional behavior is minimized.

Acknowledgement

The authors would like to thank the LID&C Co., Ltd for their financial support.

Appendix A. Supplementary material

Supplementary data to this article can be found online at <https://doi.org/10.1016/j.engstruct.2019.03.107>.

References

- [1] Whittaker AS, Bertero VV, Thompson CL, Alonso LJ. Seismic testing of steel plate energy dissipation devices. *Earthquake Spectra* 1991;7(4):563–604.
- [2] Tsai KC, Chen HW, Hong CP, Su YF. Design of steel triangular plate energy absorbers for seismic-resistant construction. *Earthquake Spectra* 1993;9(3):505–28.
- [3] Niwa N, Kobori T, Takahashi M, Hatada T, Kurino H, Tagami J. Passive seismic response controlled high-rise building with high damping device. *Earthquake Eng Struct Dyn* 1995;24(5):655–71.
- [4] Chan RW, Albermani F. Experimental study of steel slit damper for passive energy dissipation. *Eng Struct* 2008;30(4):1058–66.
- [5] Benavent-Climent A, Morillas L, Vico JM. A study on using wide-flange section web under out-of-plane flexure for passive energy dissipation. *Earthquake Eng Struct Dyn* 2011;40(5):473–90.
- [6] Köken A, Köroğlu MA. Experimental study on beam-to-column connections of steel frame structures with steel slit dampers. *J Perform Constr Facil* 2013;29(2):04014066.
- [7] Teruna DR, Majid TA, Budiono B. Experimental study of hysteretic steel damper for energy dissipation capacity. *Adv Civil Eng* 2015.
- [8] Lee M, Lee J, Kim J. Seismic retrofit of structures using steel honeycomb dampers. *Int J Steel Struct* 2017;17(1):215–29.
- [9] Lee J, Kim J. Development of box-shaped steel slit dampers for seismic retrofit of building structures. *Eng Struct* 2017;150:934–46.
- [10] Lee J, Kim J. Seismic performance evaluation of moment frames with slit-friction hybrid dampers. *Earthquakes Struct* 2015;9(6):1291–311.
- [11] Kim J, Shin H. Seismic loss assessment of a structure retrofitted with slit-friction hybrid dampers. *Eng Struct* 2017;130:336–50.
- [12] Naeem A, Eldin MN, Kim J, Kim J. Seismic performance evaluation of a structure retrofitted using steel slit dampers with shape memory alloy bars. *Int J Steel Struct* 2017;17(4):1627–38.
- [13] NourEldin M, Naeem A, Kim J. Life-cycle cost evaluation of steel structures retrofitted with steel slit damper and shape memory alloy-based hybrid damper. *Adv Struct Eng* 2018.
- [14] ASCE. Seismic evaluation and retrofit of existing buildings. ASCE41-13; 2013.
- [15] Chopra AK. Dynamics of structures. Theory Appl Earthquake Eng 2017.
- [16] ANSYS Software. ANSYS Inc., Canonsburg, PA, USA.
- [17] CSI, SAP2000 v.18 Integrated Finite Element Analysis and Design of Structures. CSI Berkeley; 2018.
- [18] ATC. Seismic evaluation and retrofit of existing concrete buildings, in ATC-40. Applied Technology Council: Redwood City (CA); 1996.

- [19] FEMA. NEHRP recommended provisions for seismic regulations for new buildings and other structures; 1997.
- [20] Kim J, Kim M, NourEldin M. Optimal distribution of steel plate slit dampers for seismic retrofit of structures. *Steel Compos Struct* 2017;25(4):473–84.
- [21] PEER. Pacific earthquake engineering research center. (<https://peer.berkeley.edu/peer-strong-ground-motion-database>).
- [22] ASCE. Minimum design loads for buildings and other structures. ASCE 7-13; 2013.